Hydrogen peroxide in the marine boundary layer over the southern Atlantic during the OOMPH cruise in March 2007

Horst Fischer[1], Andrea Pozzer[1], Torsten Schmitt[1], Patrick Jöckel[2], Tim Klippel[1], Domenico Taraborrelli[1], and J. Lelieveld[1]

[1]Max Planck Institute for Chemistry, Department of Atmospheric Chemistry, Mainz, Germany
[2]Deutsches Zentrum für Luft- und Raumfahrt (DLR), Institut für Physik der Atmosphäre, Oberpfaffenhofen, Germany
Correspondence to: Horst Fischer (horst.fischer@mpic.de)

Abstract

In the OOMPH (Ocean Organics Modifying Particles in both Hemispheres) project a ship measurement cruise took place in the late austral summer from 1st to 23rd March, 2007. The French research vessel Marion Dufresne sailed from Punta Arenas, Chile (70.85°W, 53.12°S) to La Reunion island (55.36°E, 21.06°S) across the southern Atlantic Ocean. In-situ measurements of hydrogen peroxide, methylhydroperoxide and ozone were performed and are compared to simulations with the atmospheric chemistry global circulation model EMAC. The model generally reproduces the measured trace gas levels, but underestimates hydrogen peroxide mixing ratios at high wind speeds, indicating too strong dry deposition to the ocean surface. An interesting feature during the cruise is a strong increase of hydrogen peroxide, methylhydroperoxide and ozone shortly after midnight off the west coast of Africa due to an increase in the boundary layer height, leading to downward transport from the free troposphere, which is qualitatively reproduced by the model.

1 Introduction

The oxidizing power of the lower atmosphere in the gas phase is defined by the concentrations of the hydroxyl radical (OH), ozone (O_3), the nitrate radical (NO_3), halogen radicals (e.g. ClO, BrO, IO) and hydrogen peroxide (H_2O_2), an important oxidizer in the liquid phase (Thompson, 1992). The dominant oxidizing agent is OH, whose primary source is the photolysis of O_3 and subsequent reaction of the formed O^1D-atom with water vapor (Levy, 1971). The major sinks of OH are reactions with carbon monoxide (CO), methane (CH_4), and volatile organic compounds

(VOC) yielding peroxy radicals (HO_2 and RO_2). The fate of these peroxy radicals strongly depends on the concentrations of nitrogen oxides (NOx, NO plus NO_2). In semi-polluted and polluted regions with NOx levels in excess of several tens of pptv, the peroxy radicals predominantly react with NO, yielding NO_2 and recycling OH. In these environments the subsequent photolysis of NO_2 yields ozone, with NOx acting as a catalyst. In low NOx environments, such as the marine boundary layer, the peroxy radicals undergo self-reactions ($HO_2 + HO_2$ and $RO_2 + HO_2$) yielding H_2O_2 and organic peroxides (e.g. CH_3OOH from methane oxidation), and also destroying ozone ($HO_2 + O_3$ and $OH + O_3$). The peroxides serve as reservoir species for the HOx (OH plus HO_2) radicals, which can be recycled by photolysis or reaction with OH. Hydrogen peroxide is also an important oxidizing agent in the liquid phase, notably of sulfur dioxide. Since many peroxides are water soluble, physical removal processes (deposition to surfaces and washout in rain events) strongly influence the oxidizing power of the lower atmosphere.

In the marine boundary layer at low NOx concentrations the concentrations of H_2O_2, ROOH and O_3 are strongly coupled, since their formation and destruction compete for the HO_x radicals. In order to model oxidation processes in this environment, formation and destruction of peroxides have to be accurately described, including the physical removal processes.

Previous measurements of peroxides (H_2O_2 and ROOH) in the marine boundary layer in the 1980s and 1990s have been summarized in the review article by Lee et al. (2000). Since this review additional observations in the marine boundary layer have been reported in the literature (Junkermann and Stockwell, 1999; Weller et al., 2000; Kieber et al., 2001; O'Sullivan et al., 2004; Chang et al., 2004; Stickler et al., 2007). These observations indicate highest mixing ratios (> 500 pptv) of H_2O_2 in the tropics (Slemr and Tremmel, 1994; Heikes et al., 1996; O'Sullivan et al., 1999; Junkermann and Stockwell, 1999; Weller et al., 2000; O'Sullivan et al., 2004) and decreasing concentrations toward higher latitudes in both hemispheres, reaching 200 – 300 pptv south of 40° in the southern hemisphere (Slemr and Tremmel, 1994; O'Sullivan et al., 1999; Junkermann and Stockwell, 1999; Weller et al., 2000; O'Sullivan et al., 2004). In general mixing ratios are about a factor of two higher in the northern hemisphere than at corresponding latitudes in the south (O'Sullivan et al., 1999). A significant dissimilarity between the different ocean basins has not been observed, while higher H_2O_2 mixing ratios have been observed in continental outflow (e.g. Heikes et al., 1996).

The mixing ratios of the most abundant organic peroxide CH_3OOH show similar behavior as H_2O_2 in the marine boundary layer, with highest levels in the tropics and decreasing towards the poles. Also the absolute mixing ratios are comparable, yielding H_2O_2/CH_3OOH ratios close to 1 in air masses not affected by recent rainout (Lee et al., 2000).

Here we describe in-situ ship-based observations of O_3, H_2O_2 and a proxy for CH_3OOH in the marine boundary layer of the southern Atlantic Ocean in the austral late summer of 2007. These measurements are compared to the atmospheric chemistry global circulation model EMAC (Jöckel et al., 2006, Jöckel et al., 2010). Section 2 describes the methods (measurement principles and model) used, while the observations and model comparisons are described and discussed in section 3. The final section summarizes the findings of this study.

2 Methods

2.1 OOMPH cruise MD160

As part of the OOMPH (Ocean Organics Modifying Particles in both Hemispheres) project a measurement cruise took place in the late austral summer from 1st to 23rd March, 2007. The French research vessel Marion Dufresne sailed from Punta Arenas, Chile (70.85°W, 53.12°S) to La Reunion island (55.36°E, 21.06°S) crossing the southern Atlantic between the east coast of South America to the southern Indian Ocean east of South Africa between 20°W, 60°S and 35°E, 35°S (Figure 1). During the first part of the cruise at high southern latitudes, cold air was encountered from the Antarctic continent. During this part of the cruise, cloud cover was extensive. Further north, temperatures increased together with solar radiation intensity and photolysis frequencies. The wind was generally from the west, with wind speeds varying between calm conditions and gale force winds up to 33 ms^{-1}. The average wind varied between more than 10 ms^{-1} during the first part and 8 ms^{-1} during the second part of the campaign (Figure 2). Details of the cruise can be found in Williams et al. (2010) and Hosaynali Beygi et al. (2011).

2.2 Trace gas measurements

Data used in this study were obtained by two in-situ instruments mounted in a temperature controlled container placed on the foredeck of the ship (see Fig. 3 in Hosaynali Beygi et al., 2011). Air was sampled from the top of an atmospheric mast (10 m above the deck, 20-25 m above the sea surface) through 17.1 m ½" Teflon tubes, shielded from sunlight by a black cover.

The inlet was designed as a bypass with a total flow of 24 slm (retention time 3.4 s) sustained by a membrane pump. From the bypass inlet small flows were directed to the in-situ instruments inside the container via short ¼" Teflon lines.

Hydrogen peroxide (H_2O_2) was measured with a commercial analyzer (AL2001 CA, Aero Laser, Garmisch Partenkirchen, Germany) based on wet chemical dual enzyme detection scheme described by Lazarus et al. (1985, 1986). Gaseous peroxides are sampled in a buffered (potassium hydrogen phthalate/NaOH) sampling solution (pH 5.8) in a glass stripping coil at a flow of 3 slm. The sampling efficiency for H_2O_2 was determined several times in the field and was always higher than 0.8. After passing the sampling coil the degassed liquid peroxide solution is divided into two channels and subsequently reacts with p-hydroxyphenyl acetic acid (POPHA) and horseradish peroxidase. The reaction with hydrogen peroxide, organic hydroperoxides and organic peroxides yields a fluorescent dye (6,6'-dihydroxy-3,3'-biphenyldiacetic acid) in stoichiometric quantities that is subsequently detected via fluorescence spectroscopy at 400-420 nm after excitation at 326 nm with a Cd ray lamp in a detection cell. Since the detection scheme is unspecific, the H_2O_2 concentration is determined from the difference of the two channels, with channel A measuring all peroxides (ROOH), while channel B measures ROOH – H_2O_2 after selective destruction of H_2O_2 via addition of catalase (efficiency > 95% as determined in the field) prior to the reaction with POPHA. Thus the difference between both channels provides the H_2O_2 concentration, while channel B provides an unspecific measurement of all organic hydroperoxides and organic peroxides. Nevertheless, assuming that methylhydroperoxide (MHP; CH_3OOH) is the most abundant organic peroxide in the remote marine boundary layer, as shown by previous measurements (e.g. Heikes et al., 1996), we obtain an upper limit assuming that ROOH consists of MHP only. The organic peroxide data is subsequently corrected for the lower sampling efficiency of CH_3OOH compared to H_2O_2. The time resolution (10–90%) of the instrument is 30 sec.

The in-field calibration of the instrument involves regular zero gas measurements (scrubbed ambient air after passage through cartridges filled with silica gel and hopcalite (Infiltec, Speyer, Germany)), liquid calibrations (liquid H_2O_2 standard of 35.5 $\mu g l^{-1}$) and gas phase calibrations with a H_2O_2 permeation tube (30% H_2O_2 in a glass flask temperature controlled to 40°C providing a calibration gas concentration of 6.38 ppbv). The detection limit of the instrument was determined from the 1σ variability of the in-field zero measurements performed every 2.5 h,

estimated at 25 pptv. The total uncertainty determined from the precision (1σ variability of 9 in-field gas phase and liquid calibrations), the uncertainty of the standard, the inlet transmission and an ozone interference correction was about 12-13 %. During the campaign the inlet transmission was determined twice by adding the gas phase standard at the top of the inlet line. Comparison of two calibrations directly in front of the analyzer yielded a transmission that decreased from 67% at the beginning of the campaign to 57% towards the end. The instrument has also been used (in combination with a constant pressure inlet) for airborne measurement of H_2O_2 in the free troposphere over the rainforest in South America (Stickler et al., 2007) and over Europe (Klippel et al., 2011).

A discussion of uncertainties of the MHP measurements can be based on extreme cases (all ROOH is MHP vs. no MHP at all). The model analysis on ROx radicals presented in Hosaynali Beygi et al. (2011) indicates that no other organic peroxy radicals other than CH_3O_2 are expected in the very clean marine boundary layer, indicating that MHP dominates the ROOH signal of the analyzer. A sampling efficiency of 60 % for MHP is a reasonable assumption. The efficiency cannot be higher than that for H_2O_2 (95 %) and is unlikely smaller than 30 %, thus yielding an uncertainty of ± 30 %. One should also mention that catalase reacts to some extend with MHP. The commercial analyzer (AERO-Laser, Model AL 2001CA) that has been used is based on the original design of Lazarus et al. (1986). As discussed in this paper, the effect of catalase destruction on MHP is estimated to be about 3 %, an order of magnitude less than the uncertainty due to the sampling issue discussed above.

The detection limit is determined from the reproducibility of the zero air measurements in both channels of the analyzer and strictly applies to the H_2O_2 channel. A rough estimate for MHP can be gained by multiplying with the sampling efficiency of 0.6, yielding a value of 40 pptv.

The instrument used to measure ozone (together with NO and NO_2) is a high resolution (1 s) and highly sensitive 3-channel chemiluminescence detector (CLD, ECO-Physics CLD 790 SR, Duernten, Switzerland). The instrument and its performance characteristics during this campaign have been described in detail in a previous publication on the NOx/O_3 photostationary state by Hosaynali Beygi et al. (2011). The total uncertainty for the O_3 channel was determined from the 2σ deviation of the in-field calibrations (ozone calibrator model TE49C, Thermo Instruments, Germany) and the accuracy of the standard, estimated at 1% (Hosaynali Beygi et al., 2011).

2.3 Atmospheric chemistry model EMAC

Simulations of trace gas mixing ratios along the ship cruise were performed using the EMAC (ECHAM/MESSy Atmospheric Chemistry) global circulation model (Jöckel et al., 2010). EMAC uses the Modular Earth Submodel System (MESSy; Jöckel et al., 2005) to link multi-institutional sub models describing atmospheric processes interacting with oceans, land and human influences. For this study EMAC was applied in the T42L90MA-resolution (2.8° x 2.8° resolution in latitude and longitude, 90 vertical levels up to 0.01 hPa), using results from the lowest model level (~30m) for comparison with measurements. The model was sampled (spatial bilinearly interpolated) along the ship track at every time step (i.e. 12 minutes) using the SD4 submodel (Jöckel et al., 2010), without any temporal interpolation. The meteorology was nudged to the operational ECMWF analysis. Tropospheric gas-phase and heterogeneous chemistry was calculated with the sub-model MECCA (Module Efficiently Calculating the Chemistry of the Atmosphere; Sander et al., 2005), aqueous-phase chemistry in cloud droplets and wet scavenging with the sub-model SCAV (Tost et al., 2006) and primary emissions and dry deposition of trace gases and aerosols with the sub-models ONLEM, OFFLEM, TNUDGE and DRYDEP (Kerkweg et al., 2006a and 2006b). Previous results of a model comparison with airborne H_2O_2 measurements in the free troposphere have been discussed in Klippel et al. (2011).

3 Results and discussion

3.1 Data processing

For the present analysis the original observations were averaged over 12 minute time intervals to be coherent with the model output time stepping. The time scale used is UTC, thus leading to deviations from solar noon of -80 min for the most westerly point (20°W) of the ship track to 140 min for the most easterly (35°E). Unfortunately due to the prevailing westerly winds the instruments often measured air polluted by the ship exhausts, notably when the wind was from the sector between 55° and 275°. This stack air contained very high concentrations of NO (up to 200 ppbv in individual plumes), leading to complete titration of O_3, while H_2O_2 was not affected at all on the short time scales involved, as has been observed previously (Weller et al., 2000). In total 53% of the observations were effected by stack emissions. Therefore we used Ox (O_3 + NO_2) for the experimental data, to deduce the original O_3 concentration that would have occurred without NO-titration to NO_2. In general, the difference between Ox and O_3 is marginal due to the very low NOx mixing ratios of less than 20 pptv in the remote marine boundary layer over the

189 southern Atlantic and less than 200 pptv east of South Africa (Hosaynali Beygi et al., 2011). Thus
190 the error in O_3 using Ox in all cases is smaller than 2 %. From the model only the original O_3 data
191 are used.
192
193 **3.2 Distribution of measured and simulated trace gases**
194 Figure 3 shows the time series for measured and simulated ozone mixing ratios. Observed O_3
195 varies between 17 and 25 ppbv, with lower values in the south-western Atlantic and higher values
196 closer to Africa. The model qualitatively reproduces this gradient with a slight tendency to
197 underestimate O_3 mixing ratios during the first part of the cruise (March 10 – March 14) and a
198 slight overestimation between March 15 and 17. During the last part of the cruise after March 17
199 both model and observations agree quite well. Overall, the mean observed and simulated O_3 are
200 20.3 ± 1.8 ppbv and 19.7 ± 2 ppbv, respectively. A least-square fit between simulated (y-axis)
201 and observed (x-axis) ozone yields a slope of 0.98 ± 0.01 and an offset of -0.43 ± 0.21 ppbv. The
202 regression coefficient R^2 is rather low (0.2). Taking into account that observed Ox measurements
203 are affected by background NO_2, the agreement between observations and model results is quite
204 satisfactorily. Observations and model results are in good agreement with observations by
205 Helmig et al. (2012) during the GasEx 2008 cruise in the southern Atlantic at 50° S between
206 65°W and 35°W in March 2008, who reported an average O_3 mixing ratio of 18.3 ppbv. Similar
207 O_3 mixing ratios of the order of 20 ppbv were also observed over the southern Atlantic, south of
208 40° S, during three Polarstern cruises in November 1990 (Slemr and Tremmel, 1994),
209 October/November 1994 (Junkermann and Stockwell, 1999) and March 1999 (Jacobi and
210 Schrems, 1999). As discussed in Lelieveld et al. (2004) seasonal variations of O_3 in the latitude
211 band between 40° and 60° S are rather small, with slightly lower values in austral summer. For
212 the period between 1977 and 2002 the calculated O_3 trend for this latitude band is 0.17 ± 0.08
213 ppbv/year (Lelieveld et al., 2004), indicating a moderate increase of approximately 1 ppbv
214 between 2002 and 2007. Based on the limited number of observations during OOMPH a
215 conclusion about the continuation of this trend is not possible.
216 Time series of measured and simulated H_2O_2 are shown in Figure 4. During the first part of the
217 cruise (March 10 to 14) observed H_2O_2 mixing ratios indicate small variability at levels between
218 200 and 300 pptv. During this period the model significantly underestimates observed H_2O_2, by
219 more than a factor of two. After March 14 in the eastern part of the South Atlantic H_2O_2 mixing
220 ratios tend to increase both in the observations and the model simulations, with the model

overestimating observations during the first part, in particular on March 15, while later on measurements and model results agree quite well. A period of relatively high H_2O_2 (in excess of 1 ppbv) was observed and simulated after midnight on March 16, southwest of the African coast (see Figure 1). On average observed and simulated H_2O_2 were 350 ± 220 pptv and 310 ± 240 pptv, respectively. Slope and intercept of a least-square regression analysis are 2.04 ± 0.04 and -0.27 ± 0.04 ppbv, respectively. The regression coefficient R^2 is 0.46. The imperfect agreement here between model results and observations is due to the rather limited dynamical range of mixing ratios and the strong offset during the first part of the cruise. This is also the case for O_3. As can be deduced from the time series (Figure 4) the model tends to reproduce trace gas levels over the Southern Atlantic. The measured H_2O_2 mixing ratios are comparable to previously reported observations south of 35°S in the Atlantic lower troposphere, being approximately 200 – 300 pptv (Slemr and Tremmel, 1994; Junkerman and Stockwell, 1999; Weller et al., 2000). Observations of CH_3OOH mixing ratios are shown in the time series in Figure 5 along with EMAC simulations. The temporal evolution is similar to H_2O_2, with low values (less than 200 pptv) during the first part of the cruise, a strong mixing ratio increase starting on midnight of March 16 and lower concentrations afterwards. The relative change is reproduced by the model, with a general tendency to overestimate CH_3OOH mixing ratios except during the period when the high peak was encountered on March 16. Average measured CH_3OOH mixing ratios are 280 ± 250 pptv, while the model calculates a mean value of 450 ± 190 pptv. The offset between model and observations is clearly shown in the least-square regression analysis that yields an intercept at 0.18 ± 0.05 ppbv and a slope of 0.37 ± 0.12 at an R^2 of 0.6. In general the observed mixing ratios are in good agreement with reported levels in the literature (Slemr and Tremmel, 1994; Junkerman and Stockwell, 1999; Weller et al., 2000).

With the exception of the mixing ratio peaks on March 16, the variability of O_3, H_2O_2 and CH_3OOH is small across the South Atlantic basin between South America and South Africa. The slightly northward orientation of the ship track results in a steady increase in temperature and photolysis rates (Hosaynali Beygi et al., 2011) leading to increasing photochemical activity that is likely responsible for the slight increase of the mixing ratios of the three species from the south-western to the north-eastern part of the South Atlantic. As shown in a backward trajectory analysis presented in Hosaynali Beygi et al. (2011) the air mass origin did not change throughout the cruise. All air masses encountered during the cruise originated in the western Antarctic

Peninsula during the preceding week and had not been in contact with land surfaces for at least 5 days.

3.3 Discussion

Based on H_2O_2 mixing ratios and the comparison between observations and model results, one can differentiate three different periods in Fig. 4: From March 10 to 14 the model significantly underestimates the H_2O_2 mixing ratios, while the agreement is much better during the final phase of the campaign (after March 17). In between these two periods H_2O_2 mixing ratios show a strong increase to well above 1 ppbv that is well reproduced by the model.

Similar behavior is also observed for ozone (Figure 3). The model also tends to underestimate O_3 mixing ratios during the early phase of the campaign, while the agreement is much better in the second half of the campaign. On the other hand, the CH_3OOH mixing ratios are almost always overestimated by the model (Figure 5). Considering the ratio between CH_3OOH and H_2O_2 there is an even stronger discrepancy (Figure 6). Over the whole campaign, the observed ratio varies between 0.5 and 1with a mean value and standard deviation of 0.8 ± 1.1, while the model predicts a time dependent ratio between 2 and 4 during the first half of the campaign and lower values, in good agreement with the observations, during the second half of the campaign. Hence one problem seems to be that the model underestimates H_2O_2 during the early phase of the campaign, due to either an underestimation of the H_2O_2 production or an overestimation of the sinks. Gas phase H_2O_2 in the marine boundary layers stems from the recombination of two HO_2 radicals. As shown by Hosaynali Beygi et al. (2011), EMAC reproduces observed HO_2 levels (observations are shown in Figure 10 and model results in Figure 11 of Hosaynali Beygi et al., 2011) during the whole campaign and indicates similar levels for HO_2 and CH_3O_2, the precursors of CH_3OOH. A scatter plot (not shown) and a regression analysis indicate that the model tends to overestimate observed HO_2 by approximately 20 % throughout the campaign (HO_2(obs) = (0.786 ± 0.004) x HO_2(model) – (0.44 ± 0.03); R^2= 0.87). The total uncertainty of the HO_2 measurements is ± 35 % (2σ) (Hosaynali Beygi et al., 2011), indicating that HO_2 observations and simulations agree within the uncertainties of the observations (a total uncertainty for the simulations is not available and not easy to derive). Thus the simulation tends to overestimate the H_2O_2 source by about 40 %, assuming that HO_2 reacts only with HO_2 and reactions with NO are negligible, which is justified by the very low NOx levels of less than 20 pptv in both observations and simulations. Given that the precursor levels are slightly overestimated by EMAC, it is very unlikely that an

underestimation of the peroxide production is responsible for the H_2O_2 underestimation during the first half of the campaign. This indicates that the discrepancies are due to an overestimation of the H_2O_2 sinks in the model during this period. Photochemical sinks (reaction with OH and H_2O_2 photolysis) are also unlikely causes, since the model also reproduces OH concentrations (Beygi et al., 2011) and radiation intensities (not shown). The model simulations of the photochemical H_2O_2 sinks indicate that during noon the maximum contribution of H_2O_2 photolysis and reaction with OH varies between 2 % (March 11) and a maximum of 12 % (March 19). Hence the influence of the photochemical sinks on the H_2O_2 mixing ratio is marginal (setting both sinks to zero would increase the simulated H_2O_2 mixing ratios by approx. 10 %). Other sinks of H_2O_2, in particular H_2O_2 uptake on aerosols, were not considered in the model simulation and thus cannot be responsible for the underestimation of the H_2O_2 mixing ratio in the simulations. The same is true for HO_2 loss on aerosols, which was also not considered in the model simulation.

This leaves physical removal processes, such as rainout and dry deposition to the surface, as most likely causes. Although the model predicts some rain events, they are not particularly extensive during the first phase, when the problems occur. A striking observation is that the wind speeds are significantly higher during the first part of the campaign, being well above 10 m/s up to March 15 (Figure 1), while they are generally lower in the second half of the campaign. The dry deposition in EMAC (Kerkweg et al., 2006) is based on the dry deposition scheme of Ganzeveld et al. (Ganzeveld and Lelieveld, 1995, Ganzeveld et al., 1998) partly following Wesley (1989). For highly soluble species like H_2O_2 the ocean surface resistance is assumed to be negligible and the deposition velocity strongly depends on the wind speed, which determines the transfer velocity to the ocean surface. For less soluble species like O_3 and MHP the dry deposition velocity is dominated by a non-zero ocean uptake resistance (Ganzeveld and Lelieveld, 1995). The deposition velocity calculated by the model for O_3 hardly depends on the wind speed being as small as ~ 0.05 cm/s, indicating that the deposition loss is limited by the ocean uptake resistance. On the other hand, the H_2O_2 deposition velocity is a strong function of wind speed, linearly increasing from ~ 0.5 cm/s at a wind speed of 5 m/s to about 1.8 cm/s at 10 m/s. This indicates that the deposition loss for this highly soluble species is limited by the transfer velocity to the ocean surface. These values are in good agreement with those derived from airborne measurements in the marine boundary layer over the Atlantic Ocean off the coast of South America during GABRIEL 2005 (Stickler et al., 2007). Based on H_2O_2 observations and an assumed rate of entrainment from the free troposphere Stickler et al. estimated an H_2O_2

deposition velocity of 1.3 cm/s (range <0.1 to >1.8 cm/s, depending on the assumptions for the entrainment rate) at a wind speed of 6 m/s. The single column model used in the study of Stickler et al. (2007) yielded a maximum deposition velocity of 0.5 cm/s at that wind speed, which is in good agreement with the EMAC results. Accordingly, due to the absence of low clouds and precipitation during the campaign (for the considered period) dry deposition is the dominant loss process for H_2O_2 in the model, even during the day. During the night dry deposition is the only loss mechanism, as photochemical destruction ceases. The model indicates that during daytime the contribution of dry deposition to total H_2O_2 loss varies between 98 % (noon values) during the first part of the campaign (March 11th to 14th) and about 90 % during the second half (after March 15), due to a combination of decreasing dry deposition loss due to decreasing wind speeds and a simultaneous increase by enhanced photochemical activity at lower latitudes. We performed a sensitivity study (SR1) with EMAC, limiting the maximum wind used in the deposition calculation to 5m/s, resulting in a maximum deposition velocity of H_2O_2 of around 0.6 cm/s. The green line in Figure 4 shows that this leads to an increase in simulated H_2O_2 mixing ratios by approximately 50 % (mean calculated mixing ratio: 460 ± 350 pptv). It should be mentioned that globally this effect is strongest in the marine boundary layer in regions of high wind speed, notably in the latitude band between 40° and 60° of the storm tracks in both hemispheres. Outside of these regions the effect is much smaller and leads to increases in the H_2O_2 mixing of less than 20%. Thus it appears that the differences between model simulations and H_2O_2 observations are due to a model overestimation of dry deposition to the ocean at high wind speed. This hardly affects CH_3OOH and O_3 whose deposition loss is limited by their solubility and thus independent of wind speed, while H_2O_2 is much more strongly affected. The importance of the deposition parameterization, being a critical process in the simulation of H_2O_2 in the lower troposphere was also emphasized by Chang et al. (2004), who performed sensitivity studies with a single column model to simulate observations from PEM-Tropics B.

Another interesting feature of the H_2O_2 time series in Fig. 4 is the strong increase of H_2O_2 in the night from March 15 to 16. Shortly before midnight the H_2O_2 mixing ratio increases strongly from ~ 0.7 ppbv up to about 1.5 ppbv, and decreasing to the previous mixing ratios before noon on March 16. The sudden increase occurs together with a similar increase in CH_3OOH (Figure 5), which is qualitatively reproduced by EMAC. Since the sudden increase in H_2O_2 and CH_3OOH occurs during nighttime a photochemical source can be excluded. During this phase of the campaign the ship was south of the southern tip of Africa. One explanation for the sudden

increase could be a change in air mass origin. Heikes et al. (1996) observed a significant increase of marine boundary layer H_2O_2 mixing ratios north of 20°N in continental outflow. Trajectory calculations for the OOMPH campaign were presented in the supplements to the paper by Hosaynali Beygi et al. (2011). They indicate, however, no change in air mass origin during the period between March 15 and 17, so that this option can be dismissed.

Due to the dry deposition close to the ocean surface, both H_2O_2 and CH_3OOH are expected to exhibit an increase in mixing ratios with height. Aircraft observations over the ocean indeed show maxima of both species above the marine boundary layer (Heikes et al., 1996; O'Sullivan et al., 1999; O'Sullivan et al., 2004; Stickler et al., 2007). Thus transport from above the boundary layer can be a source of H_2O_2 and CH_3OOH for the marine boundary layer. Observations of the boundary layer height were not made during the OOMPH campaign, thus we have to rely on model results. The curtain plot in Figure 7 shows a time series of the vertical profiles for O_3 (upper panel) and H_2O_2 (lower panel). Superimposed is the temporal evolution of the boundary layer height calculated by EMAC. Note that the diurnal variation of the boundary layer height during March 17^{th} – 19^{th} is related to the proximity to the African continent. Due to the limited resolution of the model the data points here are interpolated between an oceanic and a continental grid cell, leading to a diurnal evolution of the boundary layer height that resembles that of a continental boundary layer instead of the marine boundary layer. Shortly before the event the simulation indicates a very shallow boundary layer (~ 200 m), that starts to increase around midnight on March 16^{th}. Hence the increase in H_2O_2 is related to an increase in boundary layer height, and downward mixing of air masses that have not been affected by deposition and thus having higher mixing ratios of peroxides. Thus it seems that nighttime transport of free tropospheric air into the marine boundary layer is responsible for the concentration increase during the period from March 15^{th} to 16^{th}. This vertical redistribution process should also affect other species with a positive altitude gradient, in particular ozone. Model profiles indicate that the mixing ratio gradient for O_3 is much smaller than for H_2O_2 (upper panel in Fig. 7). This is consistent with the moderate change in O_3 mixing ratios during this event.

Finally, the difference in simulated and observed absolute mixing ratios of CH_3OOH needs to be addressed. Figure 5 indicates that although the model reproduces the relative changes quite well, the absolute values are off by a factor of about 2, with the model being consistently higher. The relative difference is higher in the beginning and lower towards the end of the campaign, but the absolute difference remains about 200 pptv. There are several potential explanations for this

discrepancy. First, as mentioned in section 2.2 CH_3OOH was not directly measured, but inferred from the ROOH signal, assuming that CH_3OOH is the only organic hydroperoxide and that the sampling efficiency can be calculated according to Lee et al. (2000). An experimental verification of the sampling efficiency was not performed (contrary to H_2O_2) since no CH_3OOH gas phase source was available. If the actual sampling efficiency was lower than the calculated 60%, this could close the gap between observations and model results. Additionally, the sampling efficiency would have to be lower at the beginning of the campaign and higher later on, since a simple multiplication by a factor cannot account for the rather constant absolute difference over the campaign. Therefore, although an error in the sampling efficiency cannot be excluded, it is unlikely the only source of the discrepancy between model and observations.

As discussed above, Hosaynali Beygi et al. (2011) demonstrated that EMAC very well reproduces the HO_2 measurements made during the OOMPH cruise. Since the precursor for H_2O_2 is simulated correctly by the model, one can assume that the source strength for H_2O_2 is correctly simulated. The model predicts CH_3O_2 concentrations that are similar to HO_2, but unfortunately measurements of CH_3O_2 were not made. Thus it is not possible to validate the model predicted precursor concentrations for CH_3OOH. But as discussed in Hosaynali Beygi et al. (2011) the simulated CH_3O_2 levels are quite realistic. Recently Fittschen et al. (2014) posed that the reaction of CH_3O_2 with OH radicals at low NOx concentrations can be a significant sink of methylperoxy radicals and thus could reduce CH_3OOH formation. In a sensitivity study (SR2) this reaction was included in the chemistry code of EMAC (Bossolasco et al., 2014). Additionally, we considered that in addition to CH_3OOH the reaction of CH_3O_2 with HO_2 also produces HCHO to some extend (Ayers et al., 1997). The green line in Figure 6 indicates that including these additional reaction pathways reduces the mixing ratio of CH_3O_2 in the marine boundary layer of the South Atlantic by about 30%, yielding an average mixing ratio of 300 ± 110 pptv compared to the observed 180 ± 50 pptv. It seems that the missing reaction between CH_3O_2 and OH is responsible for a largest part of the CH_3OOH overestimation by the model, in particular during the second half of the cruise when OH concentrations are high. In general, the contribution of this reaction increases with increasing OH concentration, which leads globally to a maximum impact in the tropical lower troposphere over the Pacific and Indian Oceans. The contribution of the HCHO channel in the reaction of CH_3O_2 with HO_2 is rather constant with a branching ratio of about 10%. Nevertheless, due to the uncertainties in both measurements and modeling the explanation for the difference in CH_3OOH simulation vs. observations remains ambiguous.

By combining both the reduced H_2O_2 deposition velocity and the reduced CH_3OOH source due to the competing reaction of CH_3O_2 with OH in an additional sensitivity simulation (SR3) the simulated CH_3OOH/H_2O_2 ratio is reduced to a mean value of 1.01 ± 1.06 (green line in Figure 6), much closer to the observed value (0.8 ± 1.1).

Note that an underestimation of entrainment from the free troposphere would also explain the underestimation of the H_2O_2 (and O_3) mixing ratios during the first phase of the campaign. However, this leads to an inconsistency with the MHP data, which would be affected by the same transport. Similar to H_2O_2 and O_3, MHP mixing ratios increase with altitude and show a maximum above the boundary layer (Stickler et al., 2007, Klippel et al. 2011). Thus one would expect that a transport limitation from the free troposphere in the simulations would also produce an underestimation of the simulated MHP concentrations in the MBL, but the opposite is the case; actually the model significantly overestimates MHP. Therefore, we conclude that different processes are responsible for the temporal underestimation of H_2O_2 (during the first part of the campaign) and the time independent overestimation of MHP, as most clearly corroborated in the time series of the ratio of these two species in Figure 6.

Summary and conclusions

Hydrogen peroxide, MHP and ozone have been measured in the marine boundary layer over the South Atlantic Ocean during the austral summer in 2007. Observed mixing ratios are consistent with values reported in the literature. Simulations with the atmospheric chemistry model EMAC indicate that it qualitatively reproduces the observations very well. It also qualitatively reproduces the downward mixing of high concentrations of H_2O_2 and CH_3OOH during a nighttime increase in boundary layer height south of the African continent. Quantitatively, the model tends to underestimate H_2O_2 mixing ratios during the first part of the cruise. During this part we experienced very high wind speeds, in excess of 15 m/s. Later on during the cruise much lower wind speeds were encountered for which the model accurately reproduces observed H_2O_2 mixing ratios. A similar tendency has been observed for ozone. The most likely reason for the discrepancy is that the model parameterization of trace gas deposition to the ocean surface tends to overestimate the dry deposition loss of the soluble and reactive H_2O_2 at high wind speeds. This was confirmed by a model sensitivity study with limited (at 5 cm/s) deposition velocity. MHP, which is less soluble and reactive, is not as much of affected by dry deposition, although EMAC significantly overestimates its mixing ratio. This overestimation is rather constant over the

campaign and indicates an offset of approximately 200 pptv. The reasons for this discrepancy are not easy to identify, since the measurements provide less stringent constraints than for H_2O_2. MHP was estimated from a total ROOH signal, assuming MHP being the only ROOH component and a sampling efficiency of 60 % compared to H_2O_2. Fittschen et al. (2014) recently suggested that a competing reaction of the CH_3O_2 radicals with OH can significantly diminish the source of MHP in the marine boundary layer, in particular at the low NOx concentrations observed during OOMPH. A sensitivity study with EMAC indicates that this reaction reduces the CH_3O_2 mixing ratio by about 30 %, increasing with decreasing latitude due to the meridional gradient in OH radical concentrations. Although this is a significant change, bringing CH_3OOH closer to observations, it appears to be insufficient to fully remove the discrepancy between simulated and observed CH_3OOH mixing ratios during OOMPH.

Acknowledgements: We are grateful to the OOMPH campaign (MD160) team: U. Parchatka, C. Gurk, R. Königstedt, H.D. Harder, M. Martinez, D. Kubistin, M. Rudolf, Z. Hoysaynali Beygi and J. Williams. We also thank H. Wernli for providing back trajectory data. The OOMPH project was funded under the EU sixth framework program (018419).

References

Ayers, G.P., Gillet, R.W., Granek, H., de Serves, C., and Cox, R.A.: Formaldehyde production in clean marine air, Geophys. Res. Lett., 24, 401-404, 1997.

Bossolasco, A., Farago, E.P., Schoemacker, C., and Fittschen, C.: Rate constant of the reaction between CH_3O_2 and OH radicals, Chem. Phys. Lett., 593, 7-13, 2014.

Chang, W., Lee, M., and Heikes, B.G.: One-dimensional photochemical study of H_2O_2, CH_3OOH, and HCHO in the marine boundary layer during Pacific Exploratory Mission in the Tropics (PEM-Tropics) B, J. Geophys. Res., 109, D06307, doi:10.1029/2003JD004256, 2004.

Fittschen, Ch., Whalley, L.K., and Heard, D.E.: The raction of CH_3O_2 radicals with OH radicals: A neglected sink in the remote atmosphere, Environm. Sci. & Technol., 48, 7700-7701, doi:10.1021/es502481q, 2014.

Ganzeveld, L., and J. Lelieveld, J.: Dry deposition parameterization in a chemistry general circulation model and its influence on the distribution of reactive trace gases, J. Geophys. Res., 100, 20,999-21,012, 1995.

Ganzeveld, L., Lelieveld, J., and Roelofs, G.-J.: Dry deposition parameterization of sulfur oxides in a chemistry and general circulation model, J. Geophys. Res., 103, 5679-5694, 1998.

Heikes, B.G., Lee, M., Bradshaw, J., Sandholm, S., Davis, D.D., Crawford, J., Rodriguez, J., Liu, S., McKeen, S., Thornton, D., Bandy, A., Gregory, G., Talbot, R., and Blake, D.: Hydrogen peroxide and methylhydrogenperoxide distributions related to ozone and odd hydrogen over the North Pacific in the fall of 1991, J. Geophys. Res., 101, 1891-1905, 1996.

Helmig, D., Lang, E.K., Bariteau, L., Boylan, P., Fairall, C.W., Ganzeveld, L., Hare, J.E., Hueber, J., and Pallandt, M.: Atmophere-ocean ozone fluxes during the TexAQS 2006, STRATUS 2006, GOMECC 2007, GasEx 2008 and AMMA 2008 crusies, J. Geophys. Res., 117, D04305, doi:10.1029/2011JD015955, 2012.

Hosaynali Beygi, Z., Fischer, H., Harder, H.D., Martinez, M., Sander, R., Williams, J., Brookes, D.M., Monks, P.S., and Lelieveld, J.: Oxidation photochemistry in the Southern Atlantic boundary layer: unexpected deviations of photochemical state, Atmos. Chem. Phys., 11, 8497-8513, doi:10.5194/acp-11-8497-2011, 2011.

Jacobi, H.-W., and Schrems, O.: Peroxyacetyl nitrate (PAN) distribution over the South Atlantic Ocean, Phys. Chem. Chem. Phys., 1, 5517-5521, 1999.

Jöckel, P., Sander, R., Kerkweg, A. Tost, H., and Lelieveld, J.: Technical note: The Modular Earth Submodel System (MESSy) – a new approach towards earth system modelling, Atmos. Chem. Phys., 5, 433-444. doi:10.5194/acp-5-433-2005, 2005.

493 Jöckel, P., Tost, H., Pozzer, A., Brühl, C. Buchholz, J., Ganzeveld, L., Hoor, P., Kerkweg, A.,
494 Lawrence, M.G., Sander, R., Steil, B., Stiller, G., Tanarthe, M., Taraborrelli, D., van Aardenne,
495 J., and Lelieveld, J.: The atmospheric chemistry general circulation model ECHAM5/MESSy1:
496 consistent simulation of ozone from the surface to the mesosphere, Atmos. Chem. Phys., 6, 5067-
497 5104, doi:10.5194/acp-6-5067, 2006.

498 Jöckel, P., Kerkweg, A., Pozzer, A., Sander, R., Tost, H., Riede, H., Baumgaertner, A., Gromov,
499 S., and Kern, B.: Development cycle 2 of the Modular Earth Submodel System (Messy 2),
500 Geoscientific Model Development, 3, 717-752, doi:10.5194/gmd-3-717-2010, 2010.

501 Junkerman, W. and Stockwell, W.: On the budget of photooxidants in the marine boundary layer
502 of the tropical South Atlantic, J. Geophys. Res., 104, 8039-8046, 1999.

503 Kerkweg, A., Buchholz, J. Ganzeveld, L., Pozzer, A., Tost H., and Jöckel, P.: Technical note: An
504 implementation of the dry removal process DRY DEPosition and SEDImentation in the Modular
505 Earth Submodel System (MESSy), Atmos. Chem. Phys., 6, 4617-4632, doi:10.5194/acp-6-4617-
506 2006, 2006a.

507 Kerkweg, A., Sander, R., Tost, H., and Jöckel, P.,: Technical note: Implementation of prescribed
508 (OFFLEM), calculated (ONLEM), and pseudo-emissions (TNUDGE) of chemical species in the
509 Modular Earth Submodel System (MESSy), Atmos. Chem. Phys., 6, 3603-3609,
510 doi:10.5194/acp-6-3603-2006, 2006b.

511 Lelieveld, J., van Aardenne, J., Fischer, H., de Reus, M., Williams, J., and Winkler, P.: Increasing
512 ozone over the Atlantic Ocean, Science, 304, 1483-1487, 2004.

513 Levy, H. II: Normal Atmosphere: Large radical and formaldehyde concentrations predicted,
514 Science, 173, 141-143, 1971.

515 Kieber, R.J., Cooper, W.J., Willey, J.D., and Avery Jr., G.B.: Hydrogen peroxide at the Bermuda
516 Atlantic Time Series Station. Part 1: Temporal variability of atmospheric hydrogen peroxide and
517 its influence on seawater concentrations, J. Atmos. Chem., 39, 1-13, 2001.

518 Klippel, T., Fischer, H., Bozem, H., Lawrence, M.G., Butler, T., Jöckel, P., Tost, H., Martinez,
519 M., Harder, H., Regelin, E., Sander, R., Schiller, C.L., Stickler, A., and Lelieveld, J.: Distribution
520 of hydrogen peroxide and formaldehyde over central Europe during the HOOVER project,
521 Atmos. Chem. Phys., 11, 4391-4410, doi:10.5194/acp-11-4391-2011, 2011.

522 Lazarus, A.L., Kok, G.L., Gitlin, S.N., and Lind, J.A.: Automated fluorometric method for
523 hydrogen peroxide in atmospheric precipitation, Anal. Chem., 57, 917-922, 1985.

524 Lazarus, A.L., Kok, G.L., Lind, J.A., Gitlin, S.N., Heikes, B.G., and Shetter, R.E.: Automated
525 fluorometric method for hydrogen peroxide in air, Anal. Chem., 58, 594-597, 1986.

Lee, M., Heikes, B.G., and O'Sullivan, D.W.: Hydrogen peroxide and organic peroxide in the troposphere: a review, Atmos. Environm., 34, 3475-3494, 2000.

O'Sullivan, D.W., Heikes, B.G., Lee, M., Chang, W., Gregory, G.L., Blake, D.R., and Sachse, G.W.: Distribution of hydrogen peroxide and methylhydroperoxide over the Pacific and South Atlantic Oceans, J. Geophys. Res., 104, 5635-5646, 1999.

O'Sullivan, D.W., Heikes, B.G., Snow, J., Burrow, P., Avery, M., Blake, D.R., Sachse, G.W., Talbot R.W., Thornton, D.C., and Bandy, A.R.: Long-term and seasonal variations in the levels of hydrogen peroxide, methylhydroperoxide, and selected compounds over the Pacific Ocean, J. Geophys. Res., 109, D15S13, doi:10.1029/2003JD003689, 2004.

Sander, R., Kerkweg, A., Jöckel, P., and Lelieveld, J.: Technical note: The new comprehensive atmospheric chemistry module MECCA, Atmos. Chem. Phys., 5, 445-450, doi:10.5194/acp-5-445-2005, 2005.

Slemr, F. and Tremmel, H.G.: Hydroperoxides in the marine troposphere over the Atlantic Ocean, J. Atmos. Chem., 19, 371-404, 1994.

Stickler, A., Fischer, H., Bozem, H., Gurk, C., Schiller, C., Martinez-Harder, M., Kubistin, D., Harder H., Williams, J., Eerdekens, G., Yassaa, N., Ganzeveld, L., Sander, R., and Lelieveld, J.,: Chemistry, transport and dry deposition of trace gases in the boundary layer over the tropical Atlantic Ocean and the Guyanas during the GABRIEL field campaign, Atmos. Chem. Phys., 7, 3933-3956, doi:10.5194/acp-5-3933-2007, 2007.

Thompson, A.M.: The oxidizing capacity of the Earth's atmosphere: Probable past and future changes, Science, 256, 1157-1165, 1992.

Tost, H., Jöckel, P., Kerkweg, A., Sander, R., and Lelieveld, J.: Technical note: A new comprehensive SCAVenging submodel for global atmospheric modeling, Atmos. Chem. Phys., 6, 565-574, doi:10.5194/acp-6-565-2006, 2006.

Weller, R., Schrems, O., Boddenberg, A., Gäb, S., and Gautrois, M.: Meridional distribution of hydroperoxides and formaldehyde in the marine boundary layer of the Atlantic (48°N-35°S) measured during the Albatross campaign, J. Geophys. Res., 105, 14401-14412, 2000.

Wesley, M.L.: Parameterization of surface resistances to gaseous dry deposition in regional-scale numerical models, Atmos. Environm., 6, 1293-1304, 1989.

Figure captions:

Figure 1: Ship track of the Marion Dufresne over the southern Atlantic. The track is color coded with time.

Figure 2: Time series of observed and simulated temperature and wind speed.

Figure 3: Time series of observed (red) and simulated (blue) ozone mixing ratios.

Figure 4: Time series of observed (red) and simulated (blue) hydrogen peroxide mixing ratios. In green a sensitivity simulation (SR 1) of the model is shown with reduced dry deposition velocity (see text for details).

Figure 5: Time series of observed (red) and simulated (blue) methyl hydroperoxide mixing ratios. The green line shows a sensitivity simulation (SR2) including the reaction of CH_3O_2 with OH (see text for details).

Figure 6: Simulated (blue) and observed (red) CH_3OOH to H_2O_2 ratio. The green line shows a sensitivity simulation (SR3) including reduced H_2O_2 dry deposition velocity and the reaction of CH_3O_2 with OH (see text for details).

Figure 7: EMAC simulation of O_3 (top) and H_2O_2 (bottom) vertical profiles versus time. Superimposed is the height of the planetary boundary layer. The increase in boundary layer height in the night from March 15 to 16 is associated with an increase in peroxide mixing ratios.

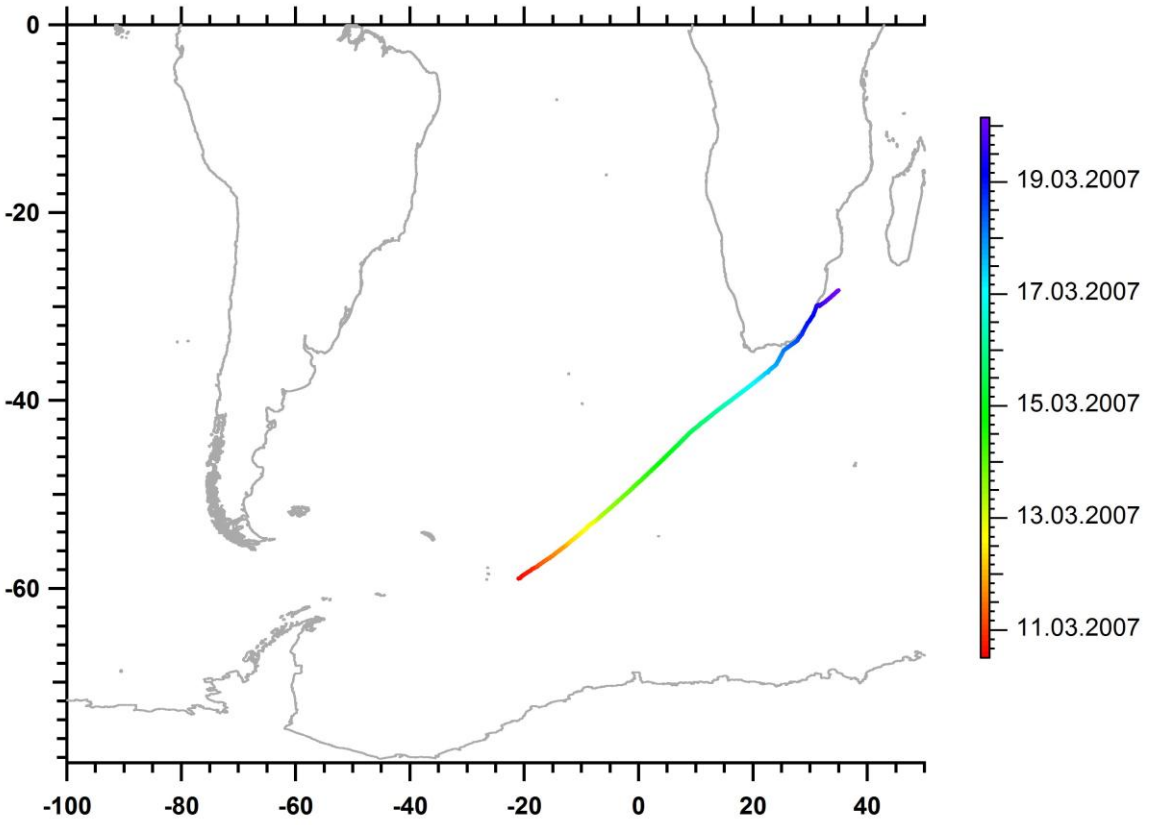

Figure 1: Ship track of the Marion Dufresne over the southern Atlantic. The track is color coded with time.

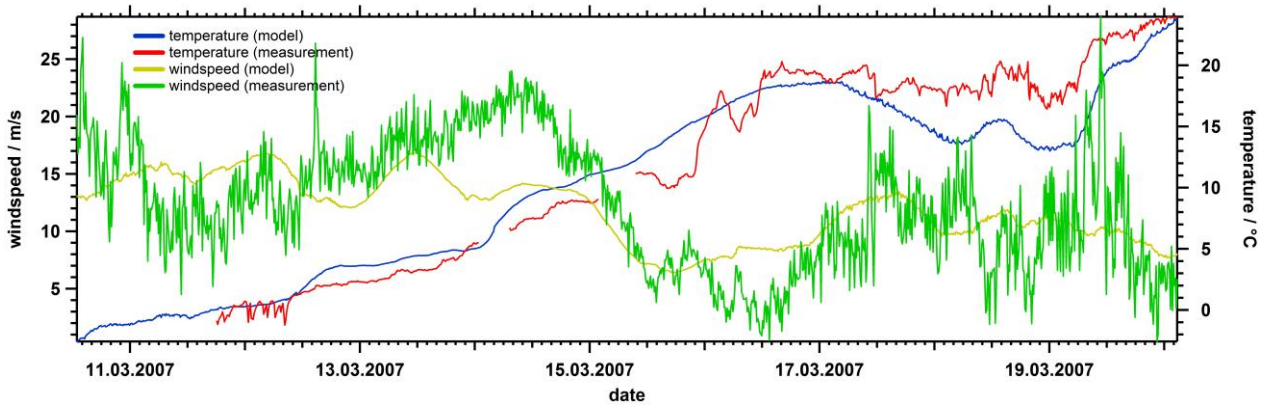

590

591 Figure 2: Time series of observed and simulated temperature and wind speed.

592

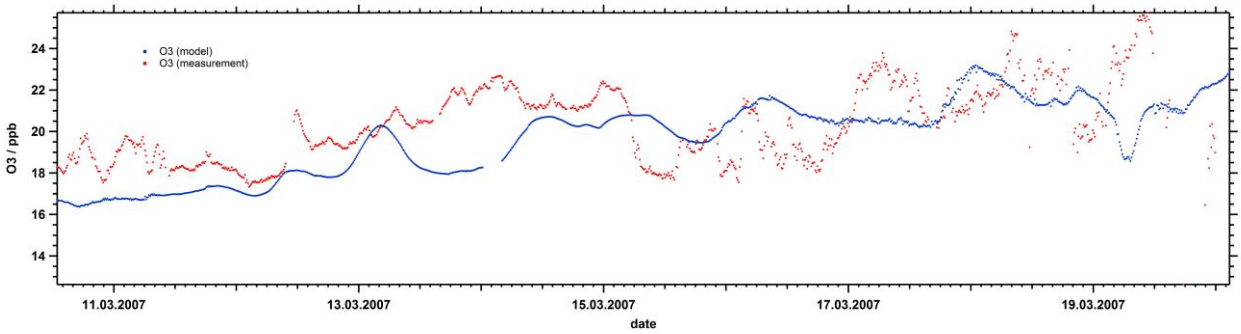

Figure 3: Time series of observed (red) and simulated (blue) ozone mixing ratios (will be revised with larger font size).

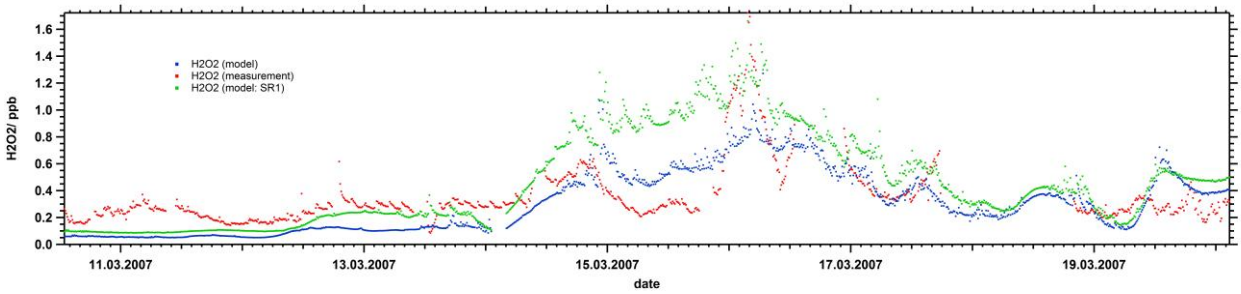

Figure 4: Time series of observed (red) and simulated (blue) hydrogen peroxide mixing ratios. In green a sensitivity simulation (SR 1) of the model is shown with reduced dry deposition velocity (see text for details) (will be revised with larger font size).

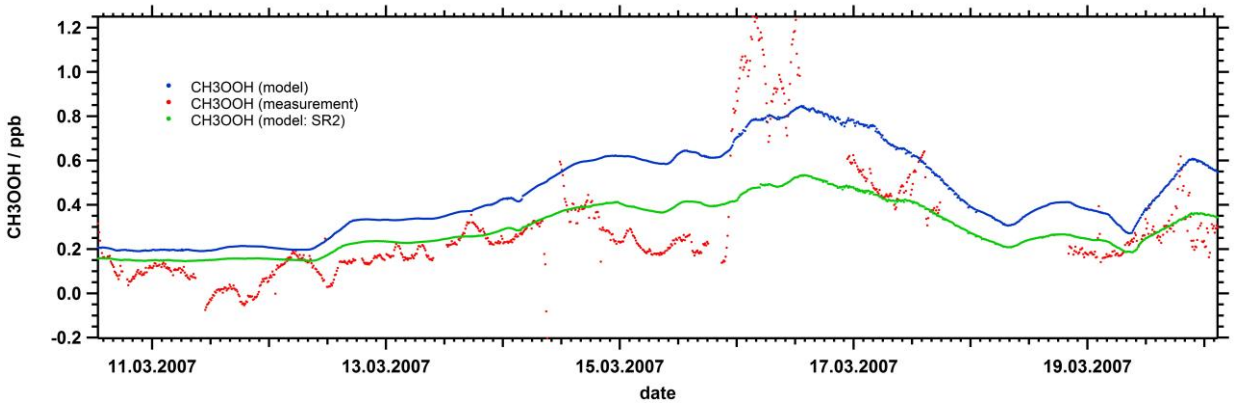

602

603 Figure 5: Time series of observed (red) and simulated (blue) methyl hydroperoxide mixing ratios.
604 The green line shows a sensitivity simulation (SR2) including the reaction of CH_3O_2 with OH
605 (see text for details).

606

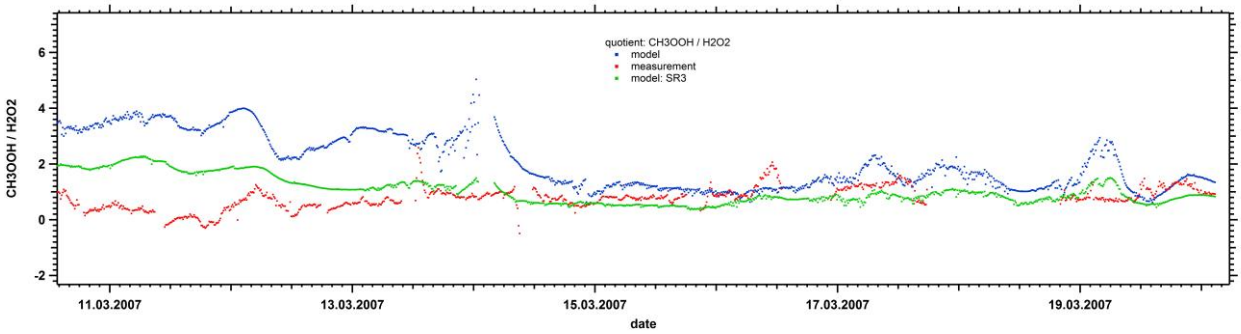

607

608 Figure 6: Simulated (blue) and observed (red) CH_3OOH to H_2O_2 ratio. The green line shows a

609 sensitivity simulation (SR3) including reduced H_2O_2 dry deposition velocity and the reaction of

610 CH_3O_2 with OH (see text for details) (will be revised with larger font size).

611

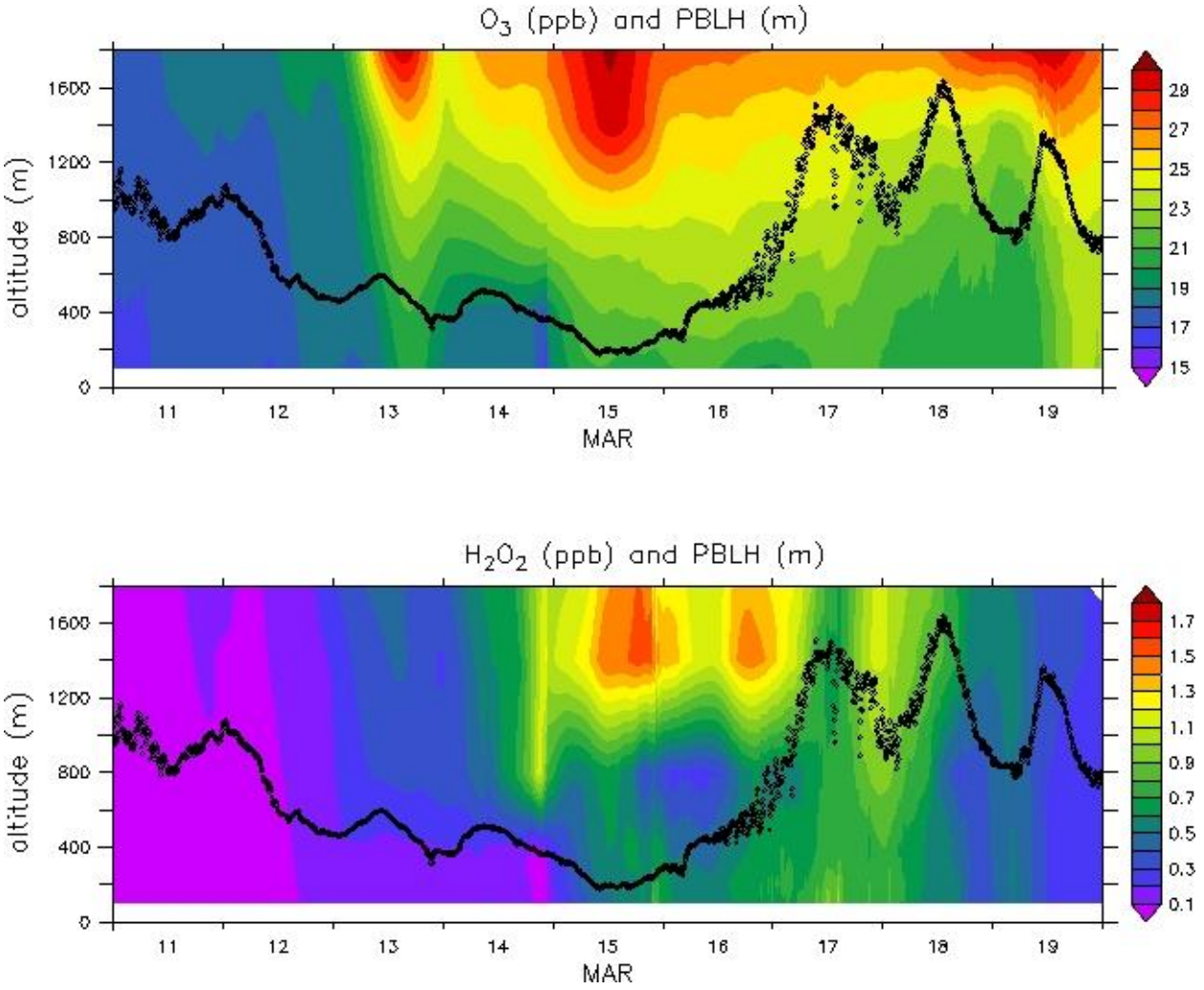

Figure 7: EMAC simulation of O_3 (top) and H_2O_2 (bottom) vertical profiles versus time. Superimposed is the height of the planetary boundary layer. The increase in boundary layer height in the night from March 15 to 16 is associated with an increase in peroxide mixing ratios.